Hindawi Publishing Corporation
EURASIP Journal on Wireless Communications and Networking
Volume 2009, Article ID 784905, 13 pages
doi:10.1155/2009/784905

*Research Article*

# Propagation Measurements and Comparison with EM Techniques for In-Cabin Wireless Networks

**Nektarios Moraitis,[1] Philip Constantinou,[1] Fernando Perez Fontan,[2] and Pavel Valtr[2]**

[1] *Mobile Radiocommunications Laboratory, National Technical University of Athens, 9 Heroon Polytechniou str., Zografou, 15773, Athens, Greece*
[2] *Department of Signal Theory and Communications, ETSI Telecommunicacion, University of Vigo, 36200, Vigo, Spain*

Correspondence should be addressed to Fernando Perez Fontan, fpfontan@tsc.uvigo.es

Received 2 September 2008; Revised 20 January 2009; Accepted 16 March 2009

Recommended by Claude Oestges

This paper presents results of a narrowband measurement campaign conducted inside a Boeing 737–400 aircraft, the objective being the development of a propagation prediction model which can be used in the deployment of in-cabin wireless networks. The measurements were conducted at three different frequency bands: 1.8, 2.1, and 2.45 GHz, representative of several wireless services. Both a simple, empirical, inverse distance power law and a deterministic, site-specific model were investigated. Parameters for the empirical model were extracted from the measurements at different locations inside the cabin: aisle and seats. Additionally, a statistical characterization of the multipath scenario created by the transmitted signal and the various cabin elements is presented. The deterministic model, based on Physical Optics (PO) techniques, provides a reasonable match with the empirical results. Finally, measurements and modeling results are provided for the penetration loss into the cabin (or out of the cabin), representative of interference scenarios.



## 1. Introduction

Airplanes seem to be the last remaining frontier where wireless communications and Internet access are still not available [1]. Airlines are increasingly interested in providing passengers with in-flight wireless services allowing a similar entertainment or business experience as their terrestrial counterparts [2]. The so-called "in-cabin wireless networks" will allow the passengers to use their own personal equipment such as mobile phones, laptops, or PDAs while the aircraft is en-route. The typical onboard infrastructure contains an in-cabin wireless access point, a service integrator/server and an aircraft-to-satellite link, in order to connect the in-cabin network to the terrestrial backbone network through a satellite, as shown in Figure 1.

To succeed in the implementation of such wireless communication systems inside aircraft, and to assess their expected performance, it is necessary to have at our disposal an in-depth and thorough characterization of the in-cabin channel. Furthermore, to avoid interference from outside networks, or interfering with external networks, it is essential to assess and limit the attenuation introduced by the body of the aircraft.

Up to now, only few measurement campaigns have been conducted in this type of scenarios, for example, [2] and [3], at very specific frequency bands. Scarce deterministic prediction and capacity planning studies [4–8] have been carried out. Simple empirical, regression-based models have been developed in [9]. As for deterministic models, they have been mainly based on (Uniform Theory of Diffraction) UTD techniques [6]. Some of the references also provide presence of passenger effects [10] and wideband measurements, that is, delays spread, not considered in this paper. Some of these studies have been performed in relation to the use of Ultra-wideband (UWB) systems [10, 11], a technique likely to be used in Wireless Personal Area Networks (WPAN) for linking computers and peripherals at very short distances.

A major concern in the use of wireless *passenger-carried electronic devices* (PEDs) aboard aircraft is their electromagnetic compatibility (EMC) with aircraft electronic systems.

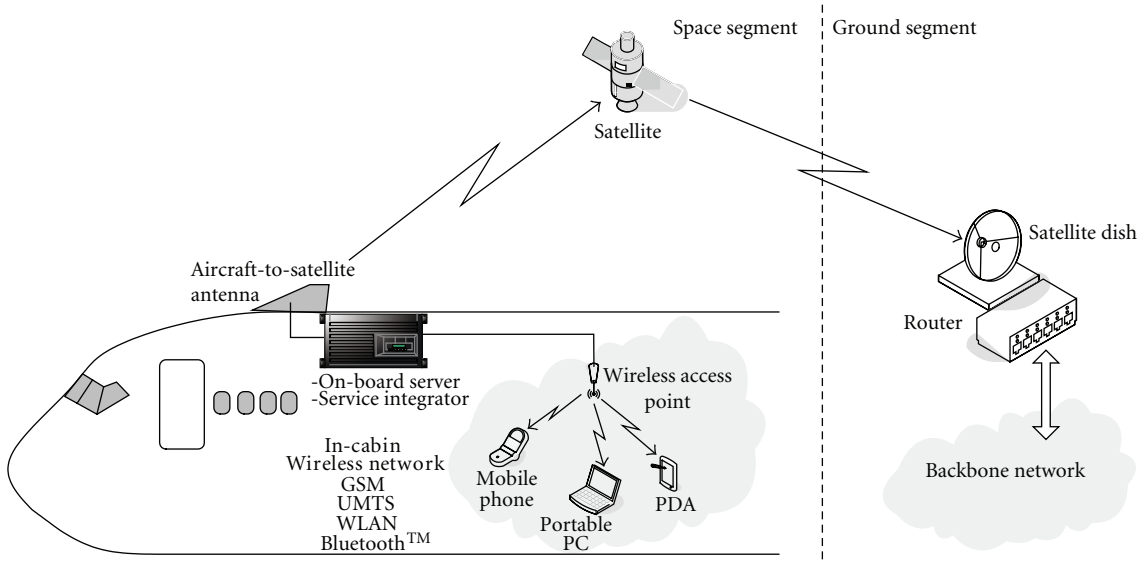


Figure 1: In-cabin wireless network infrastructure.

Intentional PED emitters are protected by frequency separation regulated by the International Telecommunication Union (ITU). Therefore, any intentional emission from an arbitrary PED is out of band for any aircraft NAV/COM system today [1]. Due to frequency separation WLAN 802.11b should not be a candidate to interfere with sensitive aircraft navigation and communication systems. WLAN is out of band to any current aircraft navigation or communication system. Consequently, Bluetooth, for example, currently is exempt from restrictions on wireless emitters inside the cabin [12]. Intentional emitters can be allowed aboard aircraft according to RTCA/DO233 recommendations if their safe use is demonstrated [13]. For A340-600 the safe use and compatibility of WLAN has been demonstrated in the aircraft environment at a power level artificially increased 250 times. Bluetooth has been investigated by Intel [14]. Lufthansa already provides a certified wireless service in the cabin in combination with portable electronic devices. During tests conducted thus far, even nonessential systems such as in-flight entertainment that are qualified to low susceptibility levels have not been observed to be disturbed [1]. From a technical point of view there is no general objection to the use of these services.

The first goal of this paper is to describe the narrowband measurement campaign performed and provide an adequate channel characterization of the in-cabin environment for personal wireless communications at GSM, UMTS, and ISM bands. This paper provides an empirical in-cabin path loss model together with a statistical characterization of the multipath environment, that is, the spatial distribution of the received signal, that is, a standing wave, complementing the results provided in the aforementioned papers. Our results refer to the aisle as well as the passenger seats. The *insertion loss* caused by the seat backrests is also defined and quantified. Additionally, *entry loss* measurements were conducted to evaluate the outdoor-to-indoor attenuation introduced by the body of the aircraft at different seats along its length.

The reported measurements were performed inside a Boeing 737–400 aircraft at three different frequency bands:

(i) 1.8 GHz representative of GSM services,

(ii) 2.1 GHz for UMTS networks,

(iii) 2.45 GHz for WLAN and Bluetooth links.

The measurements have been performed using standard antennas. An alternative to providing in-cabin coverage is using *radiating cables*, also called *leaky feeders*, laid along the roof of the cabin [3].

The second target was to develop a simple, site-specific model for in-cabin and outdoor-indoor propagation based on Physical Optics (PO) techniques. The approach followed, and the comparisons between predictions and measurements are presented in some detail. The main purpose of developing an EM based, site-specific tool is the need to extend the modeling to all possible types of aircraft. The reported measurements have been performed in a medium-sized plane. Consequently, the empirical models derived for this aircraft will not be usable in much larger airplanes, with a much larger size, and different configuration: distribution of seats, and so forth. However, once an EM model is properly validated and fine-tuned, it will be possible to use it in any new aircraft configuration, and especially, at different frequency bands that need analysis. Thus, the contribution made in this paper is expected to be of immediate practical interest.

The remainder of this paper is organized as follows. Section 2 presents the experimental setup for the in-cabin and outdoor-to-cabin measurements, a detailed description of the aircraft, and the measurement procedure are discussed. In Section 3, we show the empirical path loss model and corresponding extracted parameters from the measurement

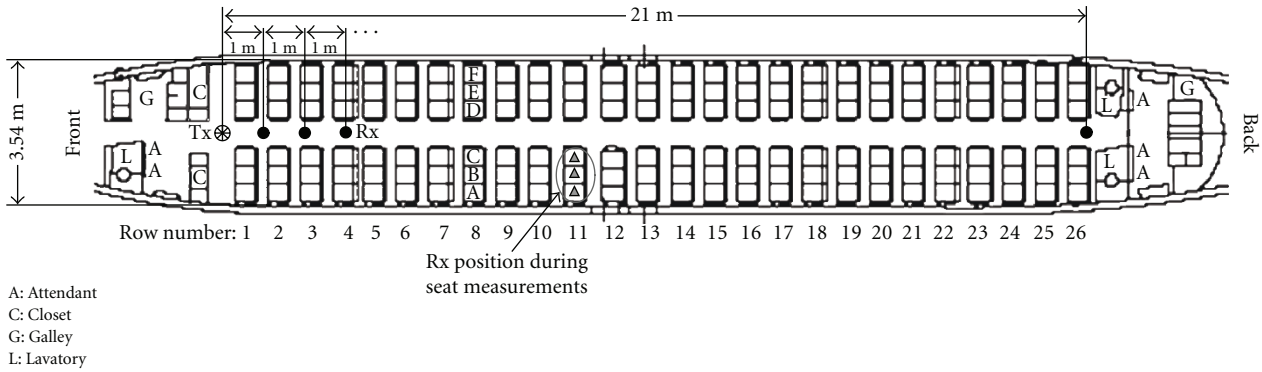


Figure 2: Ground plan of the measurement environment.

data, moreover, the fading statistics of the in-cabin radio channel are given. Additionally, the entry losses into the cabin for different locations along the length of the aircraft have also been extracted. Section 4, discusses the physical, PO-based model developed together with implementation details. A comparison between measurements and predictions is presented both for the in-cabin and penetration cases. Finally, Section 5 is devoted to summarizing the work presented in the preceding sections.

## 2. Experimental Setup

*2.1. Measurement Environment.* The Boeing 737–400 [15] is a short-haul aircraft with a seating capacity of 156 passengers, all in economy class configuration, arranged in 26 rows. The aircraft dimensions are overall aircraft length 38.4 m, height 11.15 m, maximum cabin width and height 3.54 m and 2.2 m, respectively, and length of the passengers area 22 m. Seats are called A, B, and C from window to aisle on the left side of the aisle facing the direction of flight, and D, E, and F from aisle to window on the right side of the aisle. The aisle width is 0.5 m. The seat height is 1.15 m above the floor and the distance between the seat centers is 43 cm. The distance between rows is 81 cm. The seats have textile covers. The passenger luggage compartments are located 1.68 m above the floor, 1.16 m apart, and 45 cm over the passenger heads. The ground plan of the measurement environment is shown in Figure 2.

*2.2. Measurment Setup.* The measurements were made by transmitting a continuous wave (CW) signal, at the three aforementioned frequency bands, from a fixed transmitter to a fixed receiver, and recording the signal level. The measurement setup is sketched in Figure 3. The transmitter output power was 0 dBm and antenna utilized at 1.8 GHz was a vertically polarized patch with a 7.5 dBi gain. The vertical and horizontal 3-dB beamwidths were 70° and 75°, respectively. For the measurements at 2.1 and 2.45 GHz a discone antenna with a semispherical gain of 0 dBi was used. The receive hardware was placed on a trolley, which was stationary at each measurement position. After amplification, the received signal was fed to a spectrum analyzer which was used as a receiver using the zero-span setting. The auxiliary video output of the spectrum analyzer was then sampled at 1 kHz and the values were stored to a portable PC. At the receive side, a vertically polarized omnidirectional antenna was used having a gain of between 0.75 and 1.64 dBi, depending on the frequency. The transmitter and receiver characteristics are summarized in Table 1.

Table 1: Transmitter and receiver characteristics.

| Transmitter | | | |
|---|---|---|---|
| *Frequency* | 1.8 GHz | 2.1 GHz | 2.45 GHz |
| *Power output* | | 0 dBm | |
| *Antenna gain* | 7.5 dBi | 0 dBi | 0 dBi |
| *EIRP* | 7.5 dBm | 0 dBm | 0 dBm |
| Receiver | | | |
| *Receiver sensitivity* | | −90 dBm | |
| *Antenna gain* | 1.64 dBi | 1.63 dBi | 0.75 dBi |
| *LNA gain* | 26.3 dB | 28.1 dB | 26.2 dB |
| *Total loss* | 3.7 dB | 4.7 dB | 5.3 dB |
| *Total measurable path loss* | 122 dB | 115 dB | 112 dB |

*2.3. Measurement Procedure.* Different sets of measurements were conducted inside the aircraft. In the first, the received power was measured at different points along the aisle as well as at the passenger seats in order to identify the decay rate of the average received power with increasing distances from the transmitter. Additionally, a statistical characterization of the multipath scenario, that is, its spatial variations, was also performed. Finally, the measurements have been compared with predictions carried out with a deterministic model.

During the measurements, the aircraft was in parked position and the cabin had no passengers. Under these conditions, the channel can be regarded as stationary or, at least, quasistationary. Small time variations were observed barely exceeding a standard deviation of one dB, due to the presence of the people involved in the measurements.

While performing the measurements along the aisle, the transmit and receive antennas were at 1.8 and 1.7 m above the floor, respectively, and were always aligned to point at each other, thus preserving the line-of-sight (LoS) condition. The

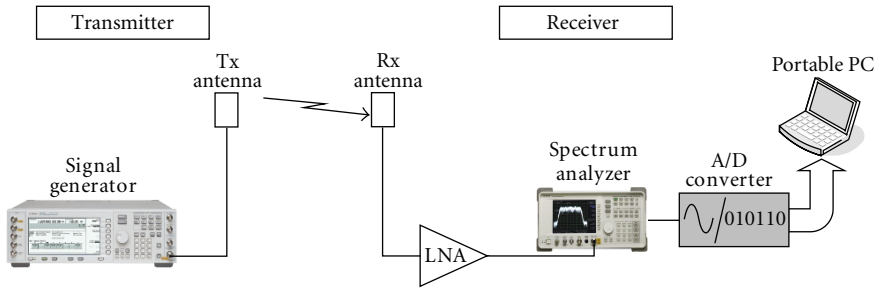


Figure 3: Measurement system setup.

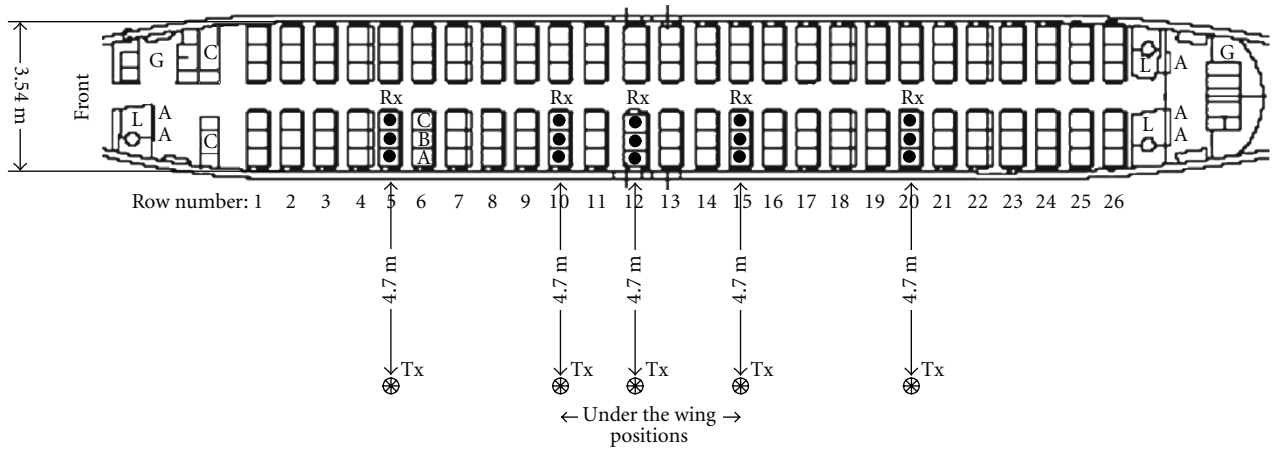


Figure 4: Ground plan of the attenuation measurement procedure.

transmitter was placed at the beginning of the aisle (Figure 2) and recordings were performed starting with the receiver located 1 m away from the transmitter up to 21 m in steps of 1 m, as indicated in Figure 2. At each position, the receive antenna was shifted by $\pm 4\lambda$ with respect to the nominal measurement position in steps of $\lambda$ (in all, 9 recordings), so as to obtain uncorrelated measurements. It should be pointed out that the spatial variations thus observed, due to a spatial standing wave generated by the multipath, are much stronger than the time variations mentioned above.

Then, the nine recordings were averaged [16]. Each recording lasted 10 seconds so that a total of 90 k samples ($9 \times 10$ s $\times$ 1000 samples/s) were used to calculate the *local mean* of the received power at each nominal measurement position. From the local mean the average path loss (dB) was calculated.

Similar measurements were also conducted at the seats. The measurements were taken at every seat from row 2 up to row 26, and at each of the three frequency bands. The transmitter was located at the same position as that given in Figure 2, at 1.8 m above the floor and the receiver was placed at each seat with the antenna a few centimeters below the head of the backrest (approximately 1.10–1.12 m above the cabin floor). Hence, the passenger seat intercepted the direct path between the transmitter and receiver, giving rise to an obstructed line-of-sight (OLoS) condition. Each recording, again, lasted 10 seconds, that is, 10 k samples which were averaged to find the mean power (*local mean*) at each passenger seat. In all, 150 sets of power recordings, corresponding to all the measurement seats, were collected (25 rows $\times$ 6 seats/row).

A final measurement set was gathered for evaluating the attenuation (*entry loss*) due to the fuselage in an outdoor-to-indoor configuration, typical of interference paths between the in-cabin network and outside networks. Attenuation measurements were taken at five different positions along the aircraft's length. The horizontal separation between the transmitter and the aircraft was always kept at 4.7 m. Attenuation measurements were taken at rows 5, 10, 12, 15, and 20. The measurements corresponding to rows 10, 12, and 15 were performed with the transmitter shaded by the wing, as shown in Figure 4. These measurements were performed with the transmitter outside the aircraft at the height of 1.65m above the ground.

The receiver was placed at the seats A, B, and C in order to collect the measurements as indicated in Figures 4 and 5. The receiver height was approximately 1.10–1.12 m above the floor. Each measurement lasted 10 seconds and, again, 10 k power samples were collected from which the average received power was computed. The average path loss was then calculated for each seat. From the actual geometry of the link, we calculated the distance between the transmitter and the receiver at each position.

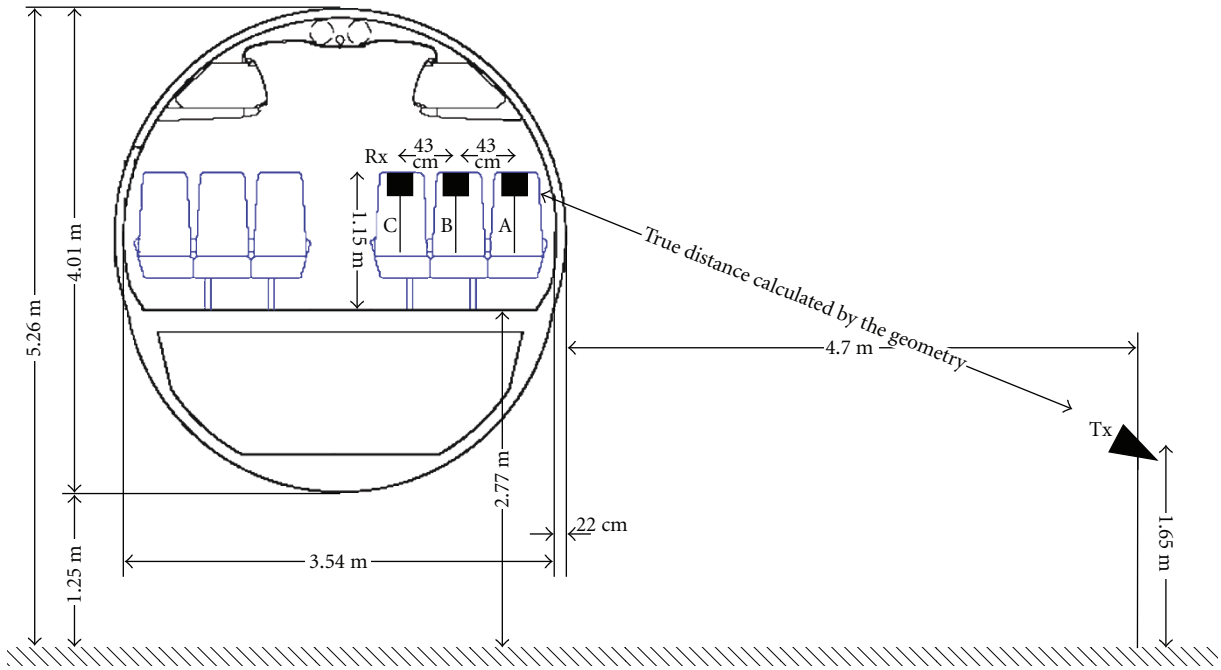


Figure 5: Cross-section of the attenuation measurement configuration.

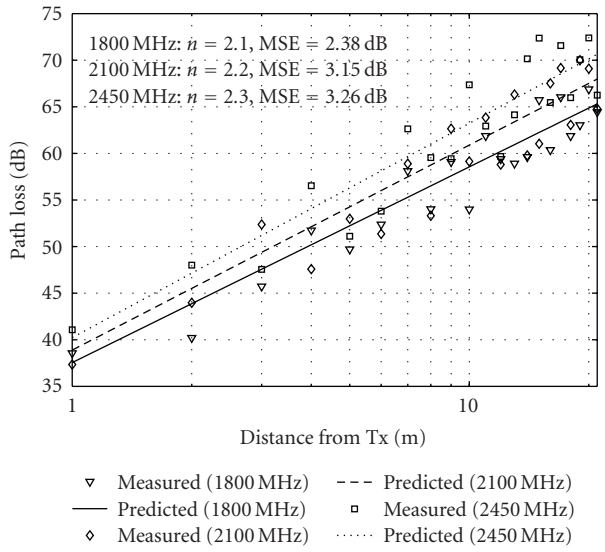


Figure 6: Path loss model results at the three frequency bands along the aisle of the aircraft.

## 3. Measurement Results

*3.1. Path Loss Modeling.* A model to predict the path loss inside the aircraft cabin, along the aisle, can be formulated using the following relationship [17]:

$$\overline{PL}(d) = FSL(d_0) + 10n \log_{10}\left(\frac{d}{d_0}\right)(\text{dB}), \qquad (1)$$

where $\overline{PL}(d)$ is the average path loss value (dB) at a distance $d$ $(m)$ from the transmitter to the receiver, $FSL(d_0)$ is the free-space path loss (dB) at a reference distance $d_0$, and $n$ is the path loss exponent (decay rate) that characterizes how fast the path loss increases with increasing transmitter-receiver separation. This model is quite standard in indoor propagation studies and corresponds, in linear units, to a power law of exponent $n$ with the inverse of the path length. What needs to be worked out is the adequate parameter, $n$, for the specific case of in-cabin propagation, where wave-guide effects may be present.

In our case, the reference distance, $d_0$, was set to 1 m, therefore, the free-space path loss is 37.5, 38.9, and 40.2 dB for 1.8, 2.1, and 2.45 GHz, respectively. Taking into account the model in (1), when performing the measurement analysis, the path loss parameter (decay rate) $n$ was found to be 2.1 at 1.8 GHz, 2.2 at 2.1 GHz and 2.3 at 2.45 GHz. The mean square error (MSE) between the measured and the predicted values was found to be 2.38, 3.15, and 3.26 dB, respectively. A comparison between the measured and the model results is presented in Figure 6 for the three bands. Given the small MSE values observed, it can be concluded that the model describes the propagation environment along the aisle with great accuracy.

Due to the specific aircraft structure (tunnel-like), path loss exponents lower than 2, indicating the presence of clear wave-guiding effects, could have been expected. In our case, the decay factor was found to be slightly greater than 2. This can be attributed to the heavy cluttered environment in the cabin. The waveguide effect is counterbalanced as the aircraft interior is comprised of materials that do not enhance the wave-guide propagation phenomenon; the floor is covered with a thick carpet while the seats are made of a non-reflective textile. Moreover, the gaps between rows of seats trap the transmitted rays, and hence, the wall-reflected power cannot fully arrive at the receiver.

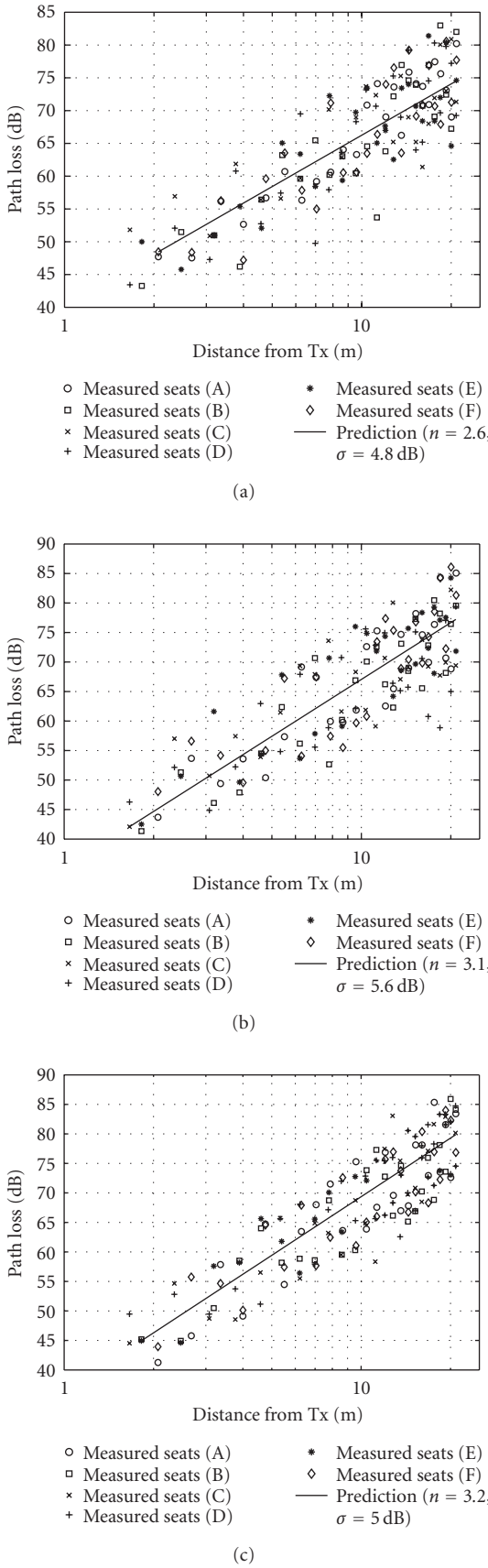


Figure 7: Path loss model results at the seats of the aircraft at: (a) 1.8 GHz, (b) 2.1 GHz, and (c) 2.45 GHz.

To describe the path loss at the seats where OLoS conditions exist, we can utilize (1) but the power decay factor is expected to be greater than 2. Applying (1) to the measured path loss at the passenger seats, the path loss exponent was found to be between 2.0 and 3.1 at 1.8 GHz, 2.5 and 3.4 at 2.1 GHz and between 2.5 and 3.9 at 2.45 GHz. The overall mean square error (MSE) between the measured and the predicted values was found to be 4.8, 5.6, and 5.0 dB, respectively.

From an ensemble study of all 150 seats, the average path loss factor, $n$, was found to be 2.6, 3.1, and 3.2 at 1.8, 2.1 and 2.45 GHz, respectively. A comparison between the measurements and the model at all the seats is presented in Figure 7 for the three frequencies. The small MSE values observed indicate that the model describes the in-cabin propagation environment with great accuracy, both at the corridor and seats.

From the measurements at the seats, we can define the *average seat insertion loss* due to the backrests. For performing such calculation, the free-space loss $FSL_i$ at each seat (150 of them) was carried out taking into account the actual Tx-Rx linear distance $d_i$. The average insertion loss was calculated using

$$\overline{L}_{seat} = \frac{1}{N}\sum_{i=1}^{N}\left(\overline{PL}_i^{\text{meas}} - FSL_i\right)(\text{dB}), \tag{2}$$

where $FSL_i$ is the free-space loss at the $i$th seat, $\overline{PL}_i^{\text{meas}}$ is the average measured path loss at the $i$-th passenger seat and $N$ is total number of measurement seats ($N = 150$). According to the above expression, the average passenger seat backrest insertion loss was 7.7 dB at 1.8 GHz, 8.1 dB at 2.1 GHz, and 9.6 dB at 2.45 GHz, respectively.

*3.2. Fading Statistics (Spatial Variability of the Channel due to Multipath).* As said in Section 2.3, the channel is practically stationary, in time, while there are very marked spatial variations due to multipath. In the measurements, it was found that the channel response remained practically constant for periods of over 7 seconds (the envelope autocorrelation function remained invariant over time at a level above 0.9), for the whole ensemble of measurement locations (aisle and seats), and of all three frequency bands.

Using the local mean of the received power as a reference, the ensemble of fade depths for a specific location was calculated as [16]

$$F_k = P_k - \overline{P}(\text{dB}), \tag{3}$$

where $F_k$ is the $k$-th fade depth (in dB), $P_k$ is the $k$th received power sample and $\overline{P}$ is the measured local mean power, both in dB. From these fade depths, the average ($M$), standard deviation ($\Sigma$), 90% percentile, minimum value, and dynamic range ($DR$) were calculated for each one of the measured locations along the aisle and at the seats. Note that one location along the corridor is actually represented by a set of nine points, including the nominal location, in a $\pm 4\lambda$ line.

Table 2, summarizes these statistical results at five different locations along the aisle at the three measurement frequencies. Additionally, Table 3 presents the average statistics for all 150 passenger seats at the three frequencies.

Table 2: Fading statistics along the aisle of the Boeing 737–400.

| $f$ [GHz] | $d_{\text{Tx-Rx}}$ [m] | $\overline{P}$ [dBm] | $\overline{PL}$ [dB] | $M$ [dB] | $\Sigma$ [dB] | 90% [dB] | min$\{F_i\}$ [dB] | $DR$ [dB] | $K$-factor [dB] |
|---|---|---|---|---|---|---|---|---|---|
| 1.8 | 1 | −6.7 | 38.5 | −0.25 | 1.07 | 1.37 | −3.7 | 4.9 | 13.6 |
| | 5 | −8.4 | 40.1 | −0.28 | 1.14 | 1.40 | −4.3 | 5.9 | 13.1 |
| | 10 | −13.9 | 45.6 | −0.30 | 1.21 | 1.47 | −4.7 | 6.3 | 12.7 |
| | 15 | −19.9 | 51.7 | −0.32 | 1.15 | 1.50 | −4.5 | 6.9 | 12.2 |
| | 20 | −17.9 | 49.6 | −0.35 | 1.33 | 1.55 | −5.2 | 7.0 | 11.3 |
| | | Overall average | | −0.30 | 1.18 | 1.46 | −4.5 | 6.2 | 12.6 |
| 2.1 | 1 | −12.3 | 37.3 | −0.30 | 1.13 | 1.41 | −4.3 | 5.6 | 13.5 |
| | 5 | −18.9 | 44.0 | −0.32 | 1.21 | 1.47 | −4.7 | 6.3 | 12.9 |
| | 10 | −27.3 | 52.4 | −0.36 | 1.33 | 1.52 | −5.1 | 6.7 | 12.3 |
| | 15 | −22.6 | 47.6 | −0.38 | 1.36 | 1.57 | −5.5 | 7.3 | 11.8 |
| | 20 | −27.9 | 53.0 | −0.40 | 1.41 | 1.63 | −5.8 | 7.8 | 11.2 |
| | | Overall average | | −0.35 | 1.29 | 1.52 | −5.1 | 6.7 | 12.3 |
| 2.45 | 1 | −19.4 | 41.1 | −0.32 | 1.22 | 1.48 | −4.9 | 6.0 | 13.8 |
| | 5 | −26.4 | 48.0 | −0.34 | 1.33 | 1.53 | −5.5 | 6.7 | 12.5 |
| | 10 | −25.9 | 47.6 | −0.37 | 1.36 | 1.59 | −6.0 | 7.7 | 12.0 |
| | 15 | −34.9 | 56.5 | −0.40 | 1.44 | 1.62 | −6.2 | 7.8 | 11.5 |
| | 20 | −29.5 | 51.1 | −0.42 | 1.51 | 1.68 | −6.3 | 8.1 | 10.9 |
| | | Overall average | | −0.37 | 1.37 | 1.58 | −5.8 | 7.2 | 12.1 |

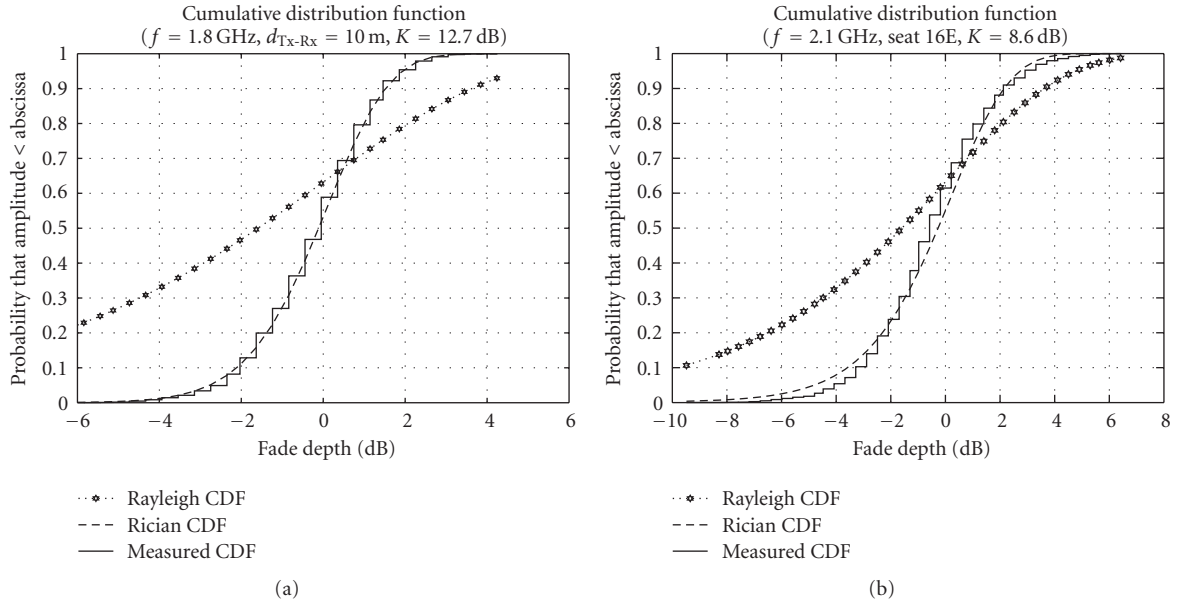


Figure 8: Indicative cumulative distribution functions: (a) at the corridor of the aircraft, and (b) at the seats of the aircraft.

Cumulative distribution functions (CDFs) for the envelope of the received signal (in linear units) were computed for each receive antenna location. In all cases, it was found that the spatial fading statistics corresponded very well with a Rice distribution with average $K$ parameter (direct-to-multipath power ratio) between 12.1 and 12.6 dB in the aisle, and between 7.3 and 8.1 dB at the seats. The Cramer-von-Mises criterion was used to estimate the goodness-of-fit [18] to the Rice distribution.

Example CDFs are presented in Figure 8 for both the aisle and the seats of the aircraft. The Rayleigh CDF is also shown for comparison. It can be observed how the $K$-factors are lower at the seats than along the aisle. This is due to obstruction of the direct ray by the backrests of the various seats.

Along the aisle, from the extracted results, only a slight increase in the dynamic range of the fades (also confirmed by the other parameters) was observed as the distance between the receiver and the transmitter was increased. However, overall, the fading statistics can be regarded as range independent. Thus, the $K$-factor only decreased with increasing distance by approximately 2 dB between first and the last sections of the measured data (Table 2).

Table 3: Average fading statistics for ensemble of seats.

| Frequency | 1.8 GHz | 2.1 GHz | 2.45 GHz |
|---|---|---|---|
| $\overline{P}$[dBm] | −33.8 | −41.0 | −45.8 |
| $\overline{PL}$[dB] | 65.6 | 66.0 | 67.5 |
| $M$ [dB] | −1.4 | −1.7 | −1.8 |
| $\Sigma$ [dB] | 2.6 | 2.8 | 2.7 |
| 90% [dB] | 2.9 | 3.1 | 2.8 |
| min$\{F_i\}$ [dB] | −11.0 | −13.5 | −14.7 |
| $DR$ [dB] | 12.6 | 15.7 | 16.3 |
| $K$-factor [dB] | 8.1 | 7.5 | 7.3 |

On the other hand, the fade dynamic range, $DR$, increases, also confirmed by the other statistics ($M$, $\Sigma$, and 90% percentile), at the seats in comparison with the results along the aisle, see Tables 2 and 3. The lower $K$-ratios at the seats, are due to the OLoS propagation condition due to the obstruction of the direct path. The received signal envelope though, still follows quite well a Rice distribution, see Figure 8(b).

From the above discussion, it is possible to complete the model in (1). This model describes the average of the path loss at distance $d$. However, a three-stage model is usually assumed when describing the actual loss [19], which includes a distance dependent term, that in (1), slow variations due to shadowing and faster (in time and space) variations due to multipath. In our case, the new expression for (1) becomes

$$PL(d) = \overline{PL}(d) + X(0,\sigma_L) + Y + Z$$
$$= FSL(d_0) + 10n\log 10\left(\frac{d}{d_0}\right) + X(0,\sigma_L) + Y + Z\,(\text{dB}), \quad (4)$$

where $PL(d)$ represents the path loss at one particular point and time which is given by the sum of an average, distance-dependent term, $\overline{PL}(d)$, a spatially slowly varying term, $X(0,\sigma_L)$, which can be modelled as a zero-mean Gaussian term with a standard deviation or location variability, $\sigma_L$, which can be equated to the MSE of the fittings in Section 3.1, that is, 2.38, 3.15, and 3.26 dB, for the aisle paths at the three frequencies of interest, and 4.8, 5.6, and 5.0 dB for the seats. The last two terms, $Y$ and $Z$, would be the space and time variability terms due to multipath. In this section we have characterized $Y$ in linear units as Rice distributed. The time variations, as said, are negligible in this case.

It should be pointed out that the measurements performed provide a limited accuracy when used for extracting passenger seat model parameters. This has been due to the fact that the measurements were taken at only one position per measurement location, that is, no spatial averaging has been carried out. However, in the time domain, variations due to the quasistatic nature of the channel have been smoothed out through time averaging of ten consecutive snapshots.

*3.3. Indoor-Outdoor Penetration Loss.* To evaluate the loss caused by the fuselage, including its openings (windows, etc.) to indoor-to-outdoor paths, we compared the free-space loss for the true distance, $d_i$, between a transmitter situated outside the aircraft and a receiver placed at seats A, B, and C, as indicated in Figure 5. Distance $d_i$ could easily be calculated using simple geometry. The attenuation for each row was calculated by averaging the measurements at seats A, B, and C according to

$$\overline{EL}_i = \overline{PL}_i^{\text{meas}} - \overline{FSL}_i\ (\text{dB}) \quad (5)$$

where $\overline{EL}_i$ is the average entry loss for row $i$, $\overline{FSL}_i$ is the average free-space loss for row $i$, and $\overline{PL}_i^{\text{meas}}$ is the average measured path loss. The data processing here also includes the averaging over all tree seats, A, B, and C, of the same row. The entry loss results are summarized in Table 4 for each frequency band. There is a clear increase in the attenuation values especially for rows 10, 12, and 15, for which the transmitter was located under the wing. On average, the attenuation was approximately 4.8 dB larger.

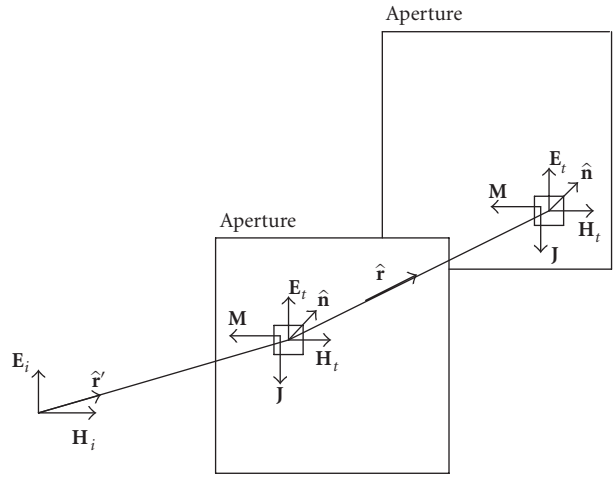


Figure 9: Basic outline of the physical optics calculation.

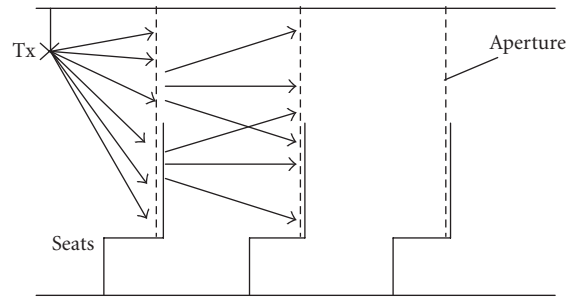


Figure 10: Schematic diagram of the modeling approach employed.

## 4. Comparison With EM Techniques

*4.1. Physical Optics Basics.* In this section, a comparison between the above measurements and simple electromagnetic modeling results based on the application of PO techniques is presented. First, we briefly describe the implementation used and, then, present the obtained results.

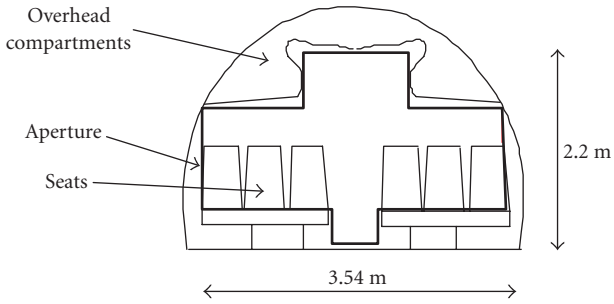


Figure 11: Cross-section of the cabin.

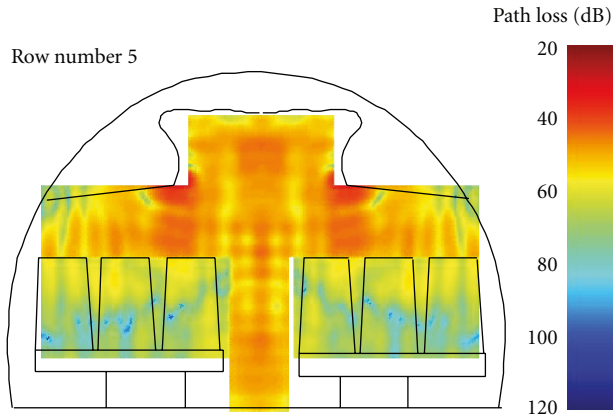


Figure 12: Example of PO results (path loss in dB) for row 5.

Table 4: Measured attenuation introduced by the haul of the aircraft.

| Frequency [GHz] | Row | $\overline{d}_{\text{Tx-Rx}}$[m] | $\overline{P}_i$[dBm] | $\overline{PL}_i^{\text{meas}}$[dB] | $\overline{FSL}_i$[dB] | $\overline{EL}_i$[dB] |
|---|---|---|---|---|---|---|
| 1.8 | 5 | 5.93 | −13.25 | 63.91 | 53.0 | 10.9 |
| | 10 | 5.92 | −18.14 | 68.80 | 53.0 | 15.8 |
| | 12 | 5.95 | −18.29 | 69.32 | 53.0 | 16.0 |
| | 15 | 5.93 | −17.87 | 68.53 | 53.0 | 15.5 |
| | 20 | 5.94 | −12.91 | 63.57 | 53.0 | 10.6 |
| 2.1 | 5 | 5.93 | −23.61 | 66.91 | 54.3 | 12.6 |
| | 10 | 5.92 | −28.86 | 72.16 | 54.3 | 17.8 |
| | 12 | 5.95 | −28.24 | 71.54 | 54.3 | 17.2 |
| | 15 | 5.93 | −28.42 | 71.72 | 54.3 | 17.4 |
| | 20 | 5.94 | −23.67 | 66.97 | 54.3 | 12.6 |
| 2.45 | 5 | 5.93 | −29.84 | 69.29 | 55.5 | 13.8 |
| | 10 | 5.92 | −34.26 | 73.71 | 55.5 | 18.2 |
| | 12 | 5.95 | −34.77 | 74.22 | 55.5 | 18.7 |
| | 15 | 5.93 | −34.53 | 73.98 | 55.5 | 18.5 |
| | 20 | 5.94 | −29.93 | 69.38 | 55.5 | 13.9 |

PO uses the concept of (equivalent) surface currents over the surface of an object or an aperture. The currents result from the overall tangential part of the incident electric and magnetic field intensity vectors. The resulting reradiated field is obtained by integrating the surface current densities over the scattering object surface [20] or, alternatively, aperture. Here, only the basic PO formulas will be presented, more details on the numerical implementation of the method can be found in [21]. It must be borne in mind that the propagation along the aircraft cabin can be calculated by considering the radiation of successive apertures. In addition, wall scattering effects can also be taken into account using PO.

The principle for the calculation of the received field strength originating at an aperture is outlined in Figure 9. The figure can be interpreted as a point source (antenna) followed by a concatenation of two apertures, each corresponding to planes where the field strength is calculated. These apertures can be taken to be along the cabin length and have the same shape as its cross-section. The apertures have to be tightly sampled in a regular mesh with a sub-lambda step. Here, for the tests carried out at 2.1 GHz ($\lambda = 0.1429$), the step size was 2 cm (14 samples per wave length).

First, the surface of all apertures has to be discretized, then the tangential components, $\mathbf{E}_t$ and $\mathbf{H}_t$, of the incident electric and magnetic fields, $\mathbf{E}_i$ and $\mathbf{H}_i$, are calculated at all points of the first aperture as

$$\begin{aligned} \mathbf{E}_t &= \hat{\mathbf{n}} \times [(\mathbf{E}_i + R\mathbf{E}_i) \times \hat{\mathbf{n}}], \\ \mathbf{H}_t &= \hat{\mathbf{n}} \times [(\mathbf{H}_i + R\mathbf{H}_i) \times \hat{\mathbf{n}}], \end{aligned} \tag{6}$$

where $R$ is the reflection coefficient which is dependent on the incidence angle and the electrical parameters of the object ($R$ is zero in the case of an aperture), and the vector cross-product with the normal to the surface, $\mathbf{n}$, represents the calculation of the tangential component.

The electric and magnetic current densities, $\mathbf{J}$ and $\mathbf{M}$, are calculated as

$$\mathbf{J} = \hat{\mathbf{n}} \times \mathbf{H}_t, \qquad \mathbf{M} = -\hat{\mathbf{n}} \times \mathbf{E}_t. \tag{7}$$

The reradiated fields, $\mathbf{E}_r$ and $\mathbf{H}_r$, at each point of the following aperture are calculated as

$$\begin{aligned} \mathbf{E}_r &= \frac{1}{4\pi} \iint_S (\hat{\mathbf{r}} \times \mathbf{M}) \frac{1 + jk_0|\mathbf{r}|}{|\mathbf{r}|} e^{-jk_0|\mathbf{r}|} dS, \\ \mathbf{H}_r &= -\frac{1}{4\pi} \iint_S (\hat{\mathbf{r}} \times \mathbf{J}) \frac{1 + jk_0|\mathbf{r}|}{|\mathbf{r}|} e^{-jk_0|\mathbf{r}|} dS, \end{aligned} \tag{8}$$

where $\mathbf{r}$ is the vector from each elementary area, $dS$, at the previous aperture to the point at the following aperture and $k_0$ is the wave number. The total electric and magnetic field, $\mathbf{E}$ and $\mathbf{H}$, at a given calculation point of the aperture is obtained as

$$\mathbf{E} = \mathbf{E}_r + Z_0 \cdot (\mathbf{H}_r \times \hat{\mathbf{r}}), \qquad \mathbf{H} = \mathbf{H}_r + \frac{1}{Z_0} \cdot (\hat{\mathbf{r}} \times \mathbf{E}_r). \tag{9}$$

*4.2. In-Cabin Propagation.* The in-cabin propagation scenario has a complex geometry, including multiple diffractions by, and multiple transmissions though, the seat backrests, and multiple reflections off the walls. Therefore, to physically model the wave propagation phenomenon within the cabin, a simplified numerical approach was attempted.

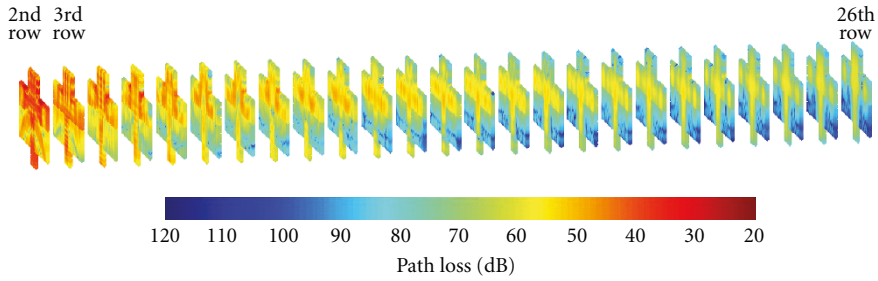


Figure 13: Example of PO results (path loss in dB) for all rows.

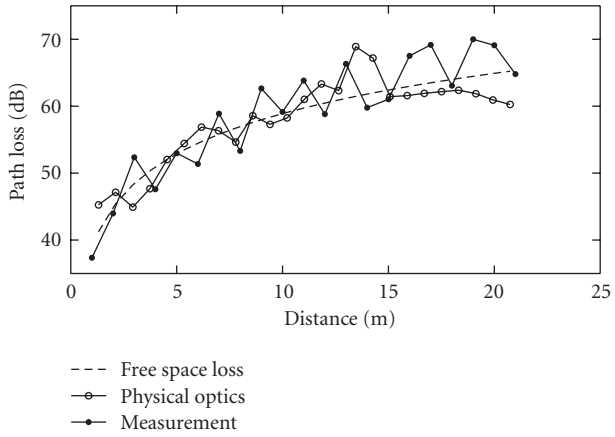


Figure 14: Comparison of simulated and measured values, aisle.

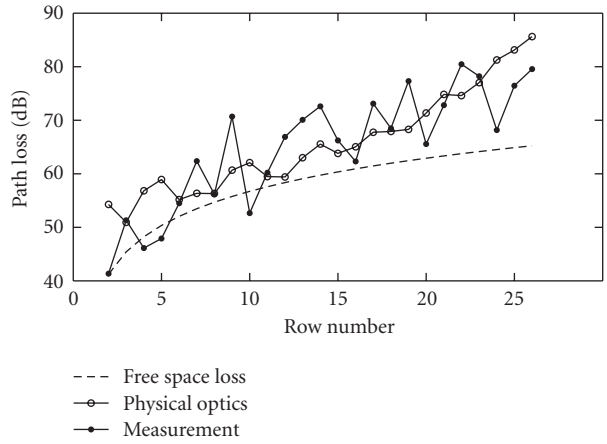


Figure 16: Comparison of simulated and measured values, B seat.

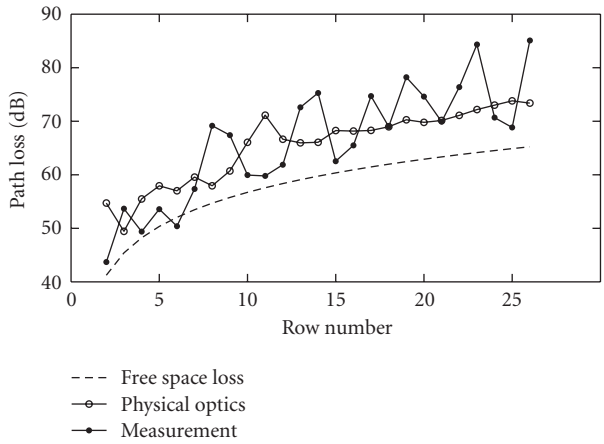


Figure 15: Comparison of simulated and measured values, A seat.

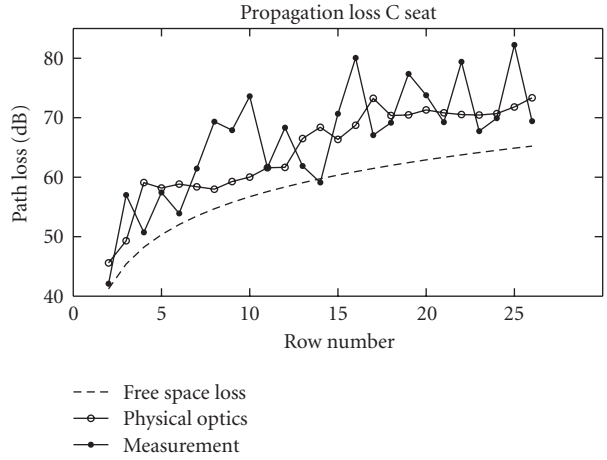


Figure 17: Comparison of simulated and measured values, C seat.

Due to the nature of the in-cabin problem, which can be decomposed into multiple screens, PO was chosen as the most suitable approach.

The field was calculated over subsequent apertures formed by the space of the cabin above the seats, by seat backrests and by the walls, the ceiling and the floor of the cabin. The field over the aperture in each row of seats is reradiated onward to obtain the field over the next aperture. This procedure is repeated for all rows. Figure 10 illustrates this approach in a schematic form. Figure 11 shows the actual cross-section of the cabin. Figures 12 and 13 show examples of obtained path loss maps. In Figure 12 the assumed simplified shape of the cabin cross-section is shown where perpendicular surfaces are considered in lieu of the actual curved ones.

The field over each subsequent aperture is calculated as a sum of the field reradiated directly from previous aperture and the contributions coming from reflections off

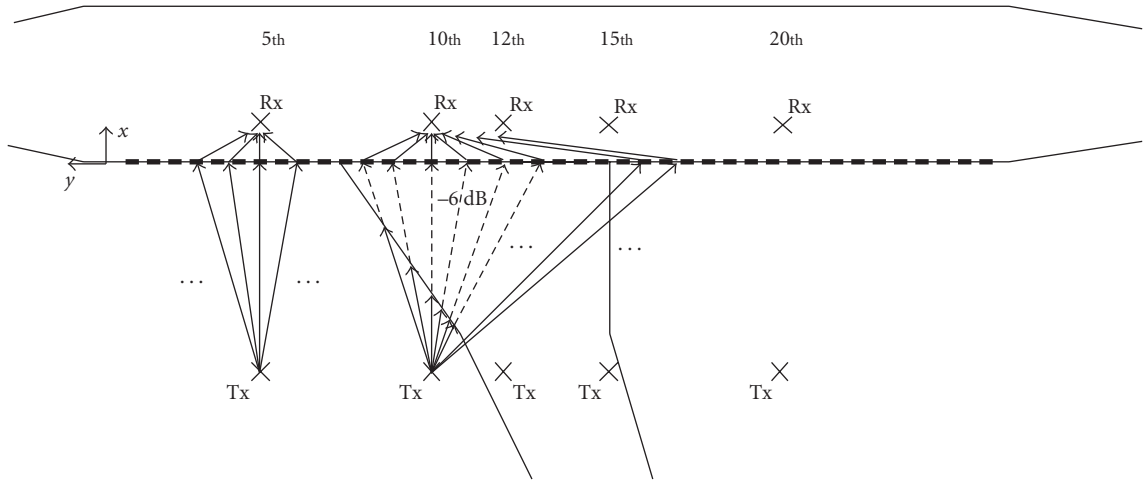


Figure 18: Received power level calculation

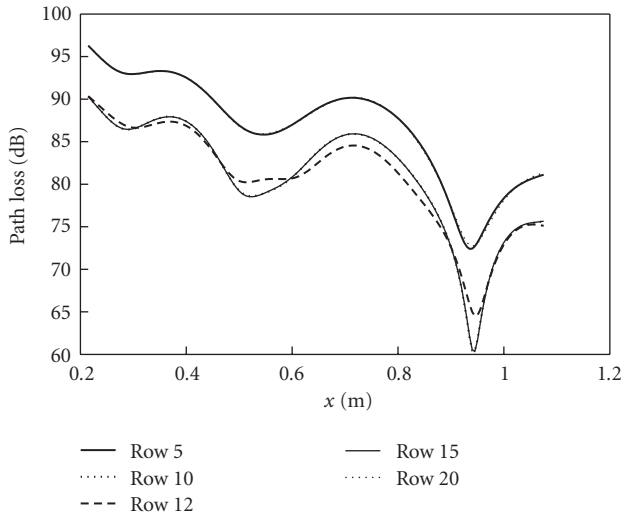


Figure 19: Propagation loss inside the cabin as a function of distance from the window.

the walls, ceiling and the floor. In all cases PO techniques were assumed.

For verifying the accuracy of the model, a vertically polarized transmitter was set in the centre of the modelled cabin at a height of 1.8 m and the frequency was 2.1 GHz. The relative permittivity and conductivity for calculating the wall reflection coefficient was $\varepsilon_r = 4$ and $\sigma = 0.03$ S/m, respectively. An additional attenuation term was added to the part of the apertures corresponding to the backrests, to account for the transmission loss. The calculation of this loss was performed assuming a 10 cm thick dielectric slab of conductivity $\sigma = 0.1$ S/m.

Figure 14 shows a comparison between the simulated and measured path loss values as the receiver is moved along the aisle at the height of 1.7 m. Figures 15, 16, and 17 show the simulated path loss at positions of the receiver 1.15 m above the floor for each seat as a function of the seat row number. The simulation results at each position have been calculated using a similar averaging process about the nominal prediction point as for the measurements. Because of the symmetry, only one side of the cabin with seats A, B, and C is shown. Note in Figure 12 the strong spatial variability of the predicted field strength. The discrepancies between measurements and predictions may be due to additional scattering effects not considered in the EM simulations. However, the simulations differ from the measurements by no more than 10 dB.

Although the simulation procedure is quite complex, several simplifications have been made. The apertures are made up of sections of rectangular shape which do not quite correspond to real cabin cross-sections. No scattering from the back and front of the cabin has been considered.

Further improvements towards a more realistic simulation of the propagation channel would mean to include additional attenuation terms due to passenger bodies, which could be modeled as lossy dielectric cuboids.

*4.3. Outdoor-to-Indoor Propagation: Entry Loss.* Also the outdoor-to-indoor case has been simulated. For a given point inside the cabin, the resulting received signal strength was calculated as a sum of the contributions from all 26 windows on the external transmitter side of the aircraft. The windows were treated as reradiation apertures using the same approach as above. The real propagation scenario shown in Figures 4 and 5 is translated into that shown in Figure 18 where the simulation approach followed is depicted.

In the case of the rows 10, 12, and 15, the contribution from each of the windows above the wing was reduced by 6 dB to account for the diffraction losses due to the shadowing by the wing. This diffraction loss introduced corresponds to that for grazing incidence on a knife-edge. From the measurements (Section 3.3) on average, the excess attenuation observed at those seats for which the transmitter was below the wing was approximately 4.8 dB larger.

Figure 19 shows the evolution of the propagation loss at 2.1 GHz as a function of the distance from the window inside the cabin for the 5th, 10th, 12th, 15th , and 20th rows.

The measured propagation losses in Table 4 are within the range of the simulated values, although the simulations show higher propagation loss as the distance from the window increases.

## 5. Conclusion

This paper presented propagation measurements and channel characterization conducted inside a Boeing 737–400. The objective was to understand the propagation mechanisms involved in the setting up of in-cabin wireless networks. The measurements were conducted in the aisle as well as at the seats at three different frequency bands (1.8, 2.1, and 2.45 GHz) representative of various different services. It has been shown how the path loss is distance dependent with additional random variations due to shadowing and multipath. Furthermore, it has been shown how the propagation exponent for aisle paths barely exceeds a value of two, close to the free-space law. This means that the expected waveguide effect which would lead to exponents below two is attenuated due to the seat rests and to the materials used that prevent the generation of strong multipath. For the seat paths, the attenuation law may be larger than three, in some cases. The spatial variations have been split into slow and fast. The slow variations can be characterized by their standard deviations, which are in the order of 3 dB for aisle paths while, for seat paths are larger, in the order of 5 dB. The faster variations have been quantified and characterized by means of Rice distributions. For interference paths between in-cabin and external networks, the excess loss with respect to free-space has been quantified, being in the order of approximately 10 to 14 dB, increasing with frequency.

The disadvantage of empirically derived models is that they are not suitable for aircraft very different from those where the measurements have been performed. The need for a generalization of results has led us to study a physical, site-specific approach. A model based on Physical (PO) techniques has been presented. Comparisons between measurement and predictions have shown a fairly good agreement. The slow received signal variations in the measurements seem to be slightly larger than in the predictions. Thin can be attributed to propagation mechanisms not considered in the modeling. Still, EM, site-specific models can provide a flexible way of producing acceptably accurate perditions for all possible aircraft configurations without the need to perform new measurements.

## Acknowledgments

The authors would like to thank the Olympic Airlines Technical Base in Athens International Airport Eleftherios Venizelos. This research has been partly carried out in the framework of the European Network of Excellence SatNEx 2.

## References

[1] A. Jahn, M. Holzbock, J. Müller, et al., "Evolution of aeronautical communications for personal and multimedia services," *IEEE Communications Magazine*, vol. 41, no. 7, pp. 36–43, 2003.

[2] N. R. Díaz and J. E. J. Esquitino, "Wideband channel characterization for wireless communications inside a short haul aircraft," in *Proceedings of the IEEE Vehicular Technology Conference (VTC '04)*, vol. 1, pp. 223–228, Milan, Italy, May 2004.

[3] N. R. Díaz, "Narrowband measurements in an airbus A319 for in-cabin wireless personal communications via satellite," in *Proceedings of the Advanced Satellite Mobile Systems (ASMS '03)*, pp. 226–233, Frascati, Italy, July 2003.

[4] G. Hankins, L. Vahala, and J. H. Beggs, "Propagation prediction inside a B767 in the 2.4 GHz and 5 GHz radio bands," in *Proceedings of the IEEE International Symposium on Antennas and Propagation Society*, vol. 1A, pp. 791–794, Chicago, Ill, USA, July 2005.

[5] G. Hankins, L. Vahala, and J. H. Beggs, "Electromagnetic propagation prediction inside aircraft cabins," in *Proceedings of the IEEE International Symposium on Antennas and Propagation Society*, vol. 3, pp. 2227–2230, Monterey, Calif, USA, June 2004.

[6] N. R. Díaz, B. S. Pérez, and F. P. Fontán, "Deterministic propagation modelling inside aircraft cabins," in *Proceedings of the 5th International Conference on ITS Telecommunications (ITST '05)*, Brest, France, June 2005.

[7] C. P. Niebla, "Topology and capacity planning for wireless heterogenous networks in aircraft cabins," in *Proceedings of the 16th IEEE International Symposium on Personal, Indoor and Mobile Radio Communications (PIMRC '05)*, pp. 2088–2092, Berlin, Germany, September 2005.

[8] C. P. Niebla, "Coverage and capacity planning for aircraft in-cabin wireless heterogeneous networks," in *Proceedings of the 58th IEEE Vehicular Technology Conference (VTC '03)*, pp. 1658–1662, Orlando, Fla, USA, October 2003.

[9] A. Kaouris, M. Zaras, M. Revithi, N. Moraitis, and P. Constantinou, "Propagation measurements inside a B737 aircraft for in-cabin wireless networks," in *Proceedings of the IEEE Vehicular Technology Conference (VTC '08)*, pp. 2932–2936, Singapore, May 2008.

[10] J. Chuang, N. Xin, H. Huang, S. Chiu, and D. G. Michelson, "UWB radiowave propagation within the passenger cabin of a Boeing 737-200 aircraft," in *Proceedings of the IEEE Vehicular Technology Conference (VTC '07)*, pp. 496–500, Dublin, Ireland, April 2007.

[11] I. Schmidt, J. Jemai, R. Piesiewicz, et al., "UWB propagation channels within an aircraft and an office building environment," in *Proceedings of the IEEE International Symposium on Antennas and Propagation and USNC/URSI National Radio Science Meeting (APSURSI '08)*, pp. 1–4, San Diego, Calif, USA, July 2008.

[12] RTCA/DO233, "Portable Electronic Devices Carried on Board Aircraft," August 1996.

[13] J. L. Schiffer and A. E. Waltho, "Intel Safety Evaluation of Bluetooth Class ISM Band Transmitters on Board Commercial Aircraft," Revision 2, December 2000.

[14] JAA TGL Leaflet No. 29, "Guidance concerning the use of portable electronic devices on board aircraft," October 2001.

[15] The Boeing, 2007, http://www.boeing.com.

[16] R. A. Valenzuela, O. Landron, and D. L. Jacobs, "Estimating local mean signal strength of indoor multipath propagation," *IEEE Transactions on Vehicular Technology*, vol. 46, no. 1, pp. 203–212, 1997.

[17] T. S. Rappaport, *Wireless Communications: Principles and Practice*, Prentice-Hall, Englewood Cliffs, NJ, USA, 1996.

[18] L. Dossi, G. Tartara, and F. Tallone, "Statistical analysis of measured impulse response functions of 2.0 GHz indoor radio channels," *IEEE Journal on Selected Areas in Communications*, vol. 14, no. 3, pp. 405–410, 1996.

[19] W. C. Y. Lee, *Mobile Communications Design Fundamentals*, Wiley Series in Telecommunications and Signal Processing, John Wiley & Sons, Chichester, UK, 1993.

[20] C. A. Balanis, *Advanced Engineering Electromagnetics*, John Wiley & Sons, New York, NY, USA, 1989.

[21] L. Diaz and T. Milligan, *Antenna Engineering Using Physical Optics: Practical CAD Techniques and Software*, Artech House, Boston, Mass, USA, 1996.